



Effects of ZnO/Mn Concentration on the Micro-structure and Optical Properties of ZnO/Mn–TiO₂ Nano-composite for Applications in Photo-Catalysis

K. Omri¹ · N. Alonizan²

Received: 8 August 2018 / Accepted: 19 September 2018 / Published online: 27 September 2018
© Springer Science+Business Media, LLC, part of Springer Nature 2018

Abstract

We successfully synthesized of ZnO/Mn–TiO₂ (Mn–Ti) nano-composite for different ZnO:Mn (Zn–M) concentrations. These composites with high photo-catalytic activity derived from TiO₂ and Zn–M nanoparticles elaborated by the sol–gel method. The SEM and TEM images indicated that samples reveals well-ordered and good size distribution of particles. In addition, the composite sample showed no aggregation in similitude with the anatase TiO₂ sample. The study of optical properties of nano-composites shows that Zn–M nanoparticles caused to increase the optical activity of Mn–Ti composites samples and it established by UV–Vis, photo-luminescence, and photo-catalytic tests. The XRD study exhibited that in ours composites samples with increasing the Zn–M concentration, the particle size increased from 10 to 27 nm. PL measurements suggest that co-emission of a strong luminescence, high yellow emission at 563 nm, at 640 nm and at 774 nm is observed from the Mn–Ti composites samples. The photo-catalytic activity of the prepared nano-composite was examined for the degradation of methyl-orange (MO) by the irradiation of UV light.

Keywords Mn–Ti nano-composite · TiO₂ · Sol–gel processes · Photo-luminescence property · Photo-catalytic property

1 Introduction

The composite nano-materials have befall very beautiful materials for industries and investigator because of their physicochemical properties such as electrical [1], optical and magnetic properties [2, 3], having diverse crystalline structure. Hence, owing to such exclusive properties of these composite new application areas is discovered in nanotechnology and industry [4]. Some common candidates, such as ZnS, ZnO, and TiO₂, have been employed as the passivation layer or shell to improve the stability of unstable photocatalyst in aqueous solution system, and their relative large band gap (3.1–3.9 eV) helps to suppress recombination of charge-carrier by constructing well-matched band

structure [3, 5]. So far, scientists have studied dielectric and structural properties of various composite materials, including anatase TiO₂ [6].

The semi-conductor materials, zinc oxide (ZnO) and TiO₂, are chemically stable with high ability to break down the bonds in the molecule [4, 6]. Also, these semi-conductor materials are not rare and expensive. Accordingly there are a lot of rapid and inexpensive various methods for preparing the nanoparticles of these nano-materials. The results of the recent research are shown that various contaminants can be destroyed by nanoparticles of ZnO and TiO₂ semi-conductor successfully [5]. Diverse researchers have elaborated composite materials through various methods, including sol–gel methods, spray pyrolysis and thermal chemical vapor deposition [6]. Xu et al. [7] elaborated ZnO/TiO₂ multilayer thin films by electron beam evaporation, and they found that this composite film showed a strong UV and violet emissions at the same time. In this regard, the use of binary metal-oxide composite materials gives another way to reduce the influence of the wide band gap and provide the capability to operate in the UV–visible spectrum [8]. Among various metal-oxide catalysts, as reported anatase TiO₂ supported Zn–M nanoparticles exhibit excellent photocatalytic performance

✉ K. Omri
omrikarim16@gmail.com

¹ Laboratory of Physics of Materials and Nanomaterials Applied at Environment (LaPhyMNE), Faculty of Sciences in Gabes, Gabes University, Gabes, Tunisia

² Department of Physics, College of Science, Imam Abdulrahman Bin Faisal University, Dammam, Saudi Arabia

[9]. Shi et al. [10] fabricated ZnO/TiO₂ thin films by E-beam evaporation, and they found that this composite film showed violet luminescence at 423 nm, rarely reported before. It is much stronger than similar luminescence reported at 420 nm. It is attributed to the interface trap in the ZnO film grain boundaries. Askari et al. [11] synthesized of TiO₂-CdS composite material by two steps for supervising the size of nanoparticles, and they found that this composite showed the photoluminescence emission involves a wide band which maximum has at 556–567 and 560 nm.

The results also compare the mechanism of ZnO doped and TiO₂ nano-materials and show that photo-catalytic characterization has been greatly enhanced by using nanoparticles. In this research nanoparticle of Zn-M and TiO₂ nanoparticles were prepared by the sol-gel method and in second step this Zn-M nanoparticles have been incorporated into TiO₂ composite. Although this synthesis was probably in one step, but these composites were elaborated in two steps to control the size of nanoparticles. The photo-catalytic activities of the synthesized Mn-Ti composite materials were investigated for decolorization of MO degradation in aqueous solution under UV light irradiation in a batch reactor. The effect of Zn-M concentrations on the photo-catalytic behaviour of Mn-Ti composite was studied in detail.

2 Experimental Procedure

The preparation of Mn-Ti nano-composite samples have been done in two steps. In the first one, Zn-M and TiO₂ nanoparticles samples elaboration process has been detailed in our previous works [12–14]. In the second step, Mn-Ti nano-composite sample with different percentages of Zn-M content 0%, 20%, 30% and 50% was prepared by solid-state reaction [14]. Finally, Mn-Ti nano-composite was obtained after annealing composite at 400 °C for 2 h under air. The crystalline phases of the samples were identified by X-ray diffraction (XRD) data of the as-produced powder samples was collected on an XRD, Model: PW-3710, diffractometer in the 2θ range from 20 to 80° with a step size of 0.02° using Cu Kα radiation with wavelength of 0.15406 nm. A LEO EVO 40xVP scanning electron microscope operated at 20 kV and equipped was used to observe the morphology of the as-manufactured samples. To study the sample morphology was analysed by transmission electron microscope (TEM) operated at 200 kV (TEM Model CM200, SUPER-TWIN). The optical propriety of the samples was determined using Shimadzu UV-3101 PC spectrophotometer and the 450-W Xenon lamp was used as an excitation source.

The photocatalytic activities of Mn-O-Ti nano-composite were evaluated using MO degradation by UV light irradiation (600 W, main wave crest at 365 nm). For comparison

of efficiency a commercially TiO₂ (Degussa P25) was tested in this study.

3 Results and Discussions

3.1 Structural and Morphological Investigation

Figure 1 shows the X-ray diffraction (XRD) pattern of Mn-Ti nano-composite samples with different Zn-M nanoparticles concentrations (0, 20, 30 and 50 at%). In the XRD patterns of our samples the diffraction peaks situated at 2-theta 25.3°, 37.8°, 48°, 53.9°, 55°, 62.56°, 68.7°, 70.15° and 75° are indexed to the following crystal plane: (101), (104), (200), (105), (211), (204), (116), (220) and (215) [15–19]. The diffraction peaks (101) and (200) of Mn00%-Ti composites can be indexed to TiO₂-anatase (tetragonal) phase (JCPDS No. 04-0477), and very good agreement with the result reported by Homann et al. [17]. Furthermore, the anatase TiO₂ it crystallizes in a tetragonal unit cell (Fig. 2), with the lattice constants $a = 3.78 \text{ \AA}$ and $c = 9.51 \text{ \AA}$. The results indicate that the sample is there is a large corresponds in the peaks of TiO₂ and ZnO in this spectrum. The XRD pattern indicates the formation of hexagonal wurtzite phase of ZnO [14, 18], were matched well with space group P63mc (No. 186) (JCPDS No. 36-1451), with formed of TiO₂. It can be seen that for the Mn-Ti nano-composite sample diffraction peaks correspond to the hexagonal ZnO materials (JCPDS No. 79-0205) (Fig. 3), the indexed to the following crystal plane: (100), (002), (101), (102), (110), (103), (200), (112) and (201), which can be assigned to diffraction from 32.6°, 34.7°, 36.5°, 47.8°, 56.8°, 63.1°, 66.6°, 68.0° and 69.3° planes respectively [19–21]. The peaks TiO₂ remained original reflections of anatase

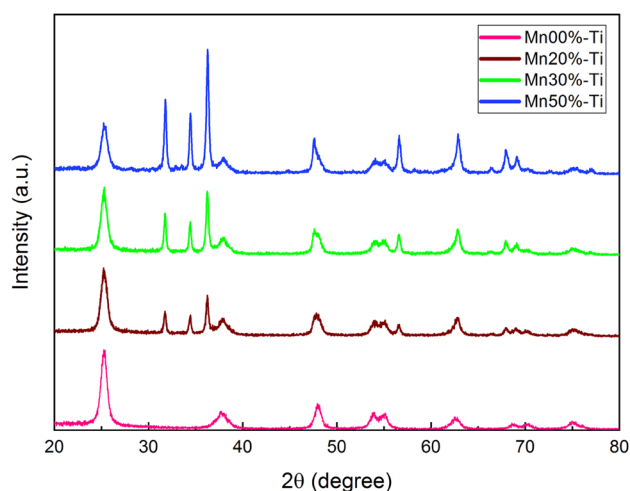


Fig. 1 X-ray diffractograms of Mn-Ti nanocomposite for different Zn-M concentrations

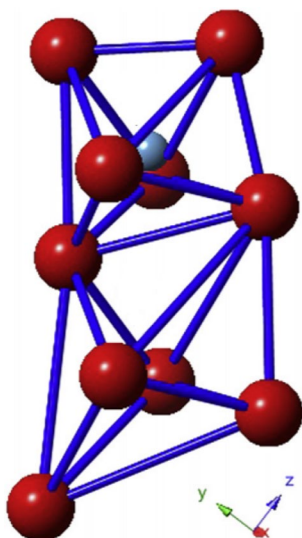


Fig. 2 Schematic representation of the in TiO_2 anatase structure [18]

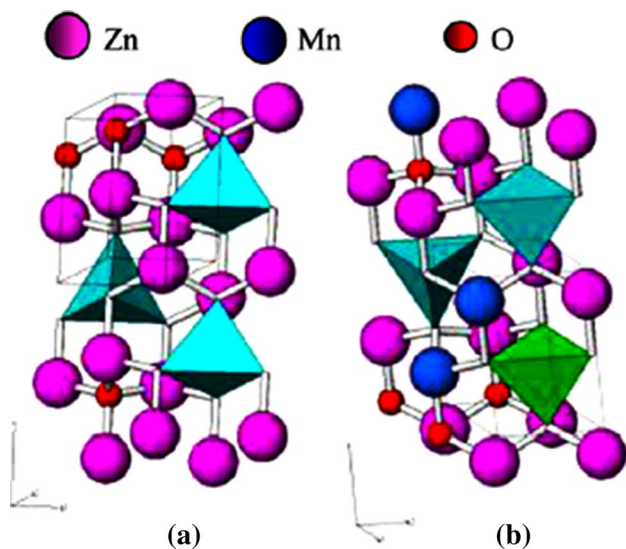


Fig. 3 Structures wurzite of a ZnO and b Zn-M [19]

crystalline phase [22]. However, diffraction peak around $2\text{-theta} = 25.20^\circ$ (110) of Mn–O–Ti nano-composites sample became weaker with an increase of Zn–M nanoparticles concentrations (20, 30 and 50 at%) and similar trends could be determined for the TiO_2 anatase peaks [23, 24]. Similarly ZnO nanoparticles remained original reflections. But diffraction peaks of Mn–Ti nano-composite sample became stronger, and the peaks of ZnO correspond (overlap) with peaks of Mn–Ti nano-composite. In other words, there is clearly no correspond (no overlap) between TiO_2 peaks with ZnO in Mn–Ti nano-composite sample and indicating the non-interference of TiO_2 nanoparticles in the crystalline structure of Zn–M nanoparticles [25]. But the effect of

increased Mn concentration appears in the lack of diffraction X-ray intensity of ZnO. The XRD patterns show increase intensity of Mn–Ti samples, so we can say that increase concentrations of Zn–M nanoparticles increase size of Mn–Ti samples. The crystallite size of Mn–Ti nano-composite samples were calculated using Scherrer's equation [26]. The average crystallite size of Mn00%–Ti particles in the range 8.4–10.4 nm, and of Mn–Ti nano-composite is increasing from 14 to 27 nm (Table 1). Mean the anatase grain size of Mn00%–Ti sample has stayed same with the increase in the Zn–M nanoparticles concentration due to the formation of Mn–Ti composite bonds, was very good agreement with the result reported by Devi et al. [27].

The SEM morphologies of Mn–Ti nano-composite samples with different Zn–M nanoparticles concentrations (00, 20, 30 and 50 at%) are shown in Fig. 4. Note that a Mn00%–Ti particles with a granular morphology can be seen clearly and Mn–Ti nano-composite have crystalline spheres–hexagonal shape and obtained is granular and well dispersed. It is also observed that Mn00%–Ti particles are main components in the Mn–Ti nano-composite samples, and Zn–M nanoparticles were dispersed on the surfaces of the obtained TiO_2 in the Mn–Ti nano-composite samples, which would be beneficial to improve the catalytic activity composite photo-catalysts in essence. Obviously, Mn doping has a remarkable effect on the particle size of Mn–Ti nano-composite samples. Where the particle size of Mn–Ti nano-composite tends to increase with increasing of concentrations percentage of Mn doping.

Figure 5 shown the TEM image of pattern of Mn–Ti nano-composite samples with different Zn–M nanoparticles concentrations (00, 20, 30 and 50 at%). TEM results showed that particle size of pure TiO_2 sample is a spherical small crystalline nanoparticle less than 10.5 nm, while, the particle sizes of the Mn20%–Ti, Mn30%–Ti and Mn50%–Ti samples are 13.98, 15.22 and 26.81 nm respectively. It is clear that the incorporation of Zn–M nanoparticles in TiO_2 for formed the Mn–Ti nano-composite induced to increase the average grain size. The increase in particle size of the Mn–Ti nano-composite system may be due to the ability of Mn ions to activate the crystal growth rate of ZnO. Substitution of Mn ions into ZnO lattice can produce some defects. Therefore, variation in defect concentration can cause a change in the

Table 1 Particle dimension (D) of Mn–Ti nanocomposite for different Zn–M concentrations

Zn–M doping concentrations (at.%)	D (nm)
0.0	10.33
20	14.20
30	15.10
50	27

Fig. 4 Typical typical SEM photograph showing (3, 10 μm) the of **a** Mn00%–Ti, **b** Mn20%–Ti, **c** Mn30%–Ti, and **d** Mn50%–Ti nano-composite

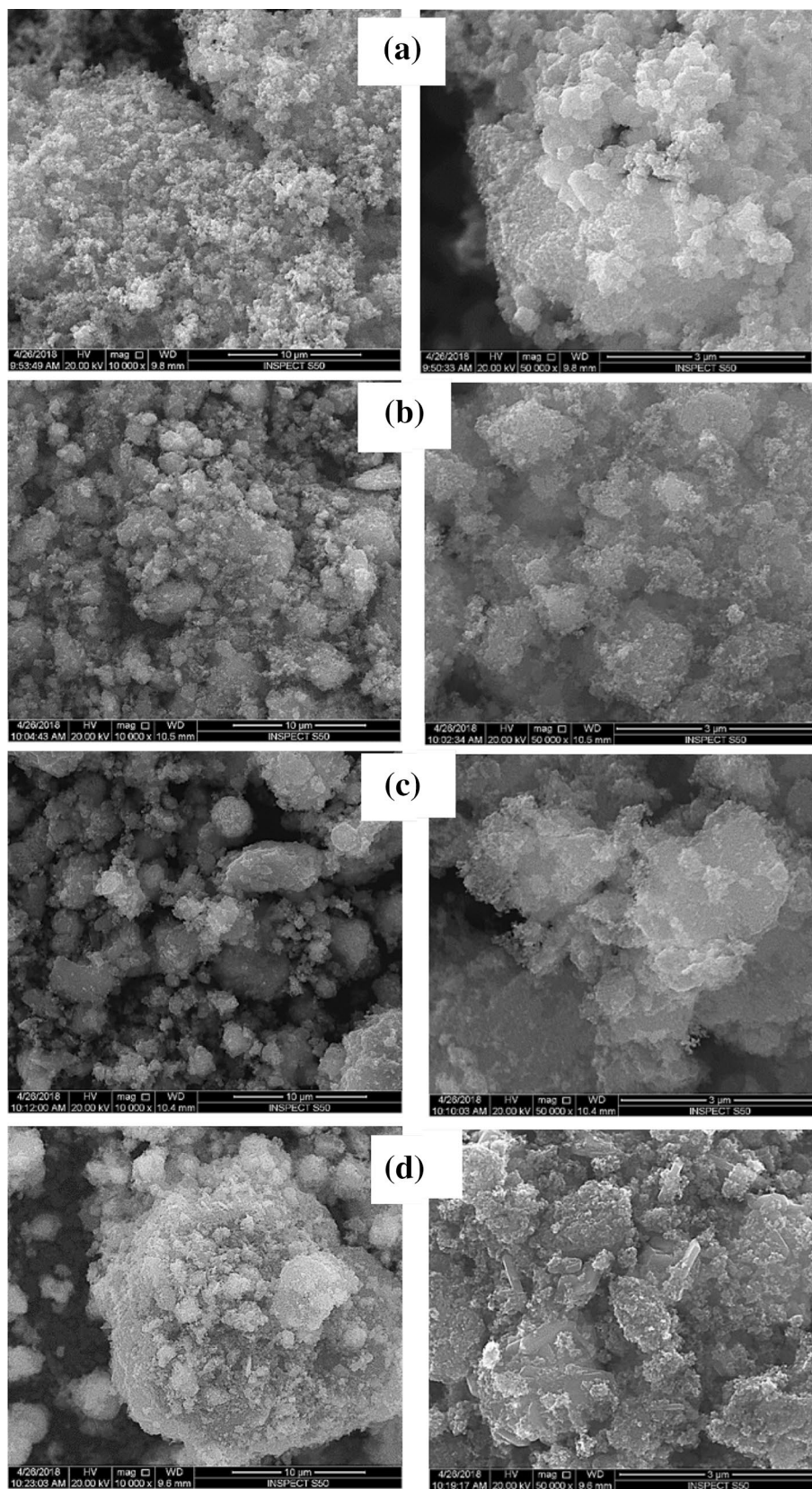


Fig. 5 Typical TEM photograph showing the general morphology of **a** Mn00%–Ti, **b** Mn20%–Ti, **c** Mn30%–Ti, and **d** Mn50%–Ti nanocomposite

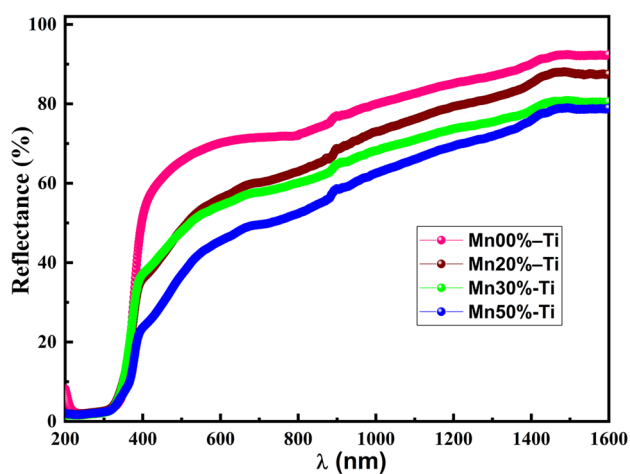
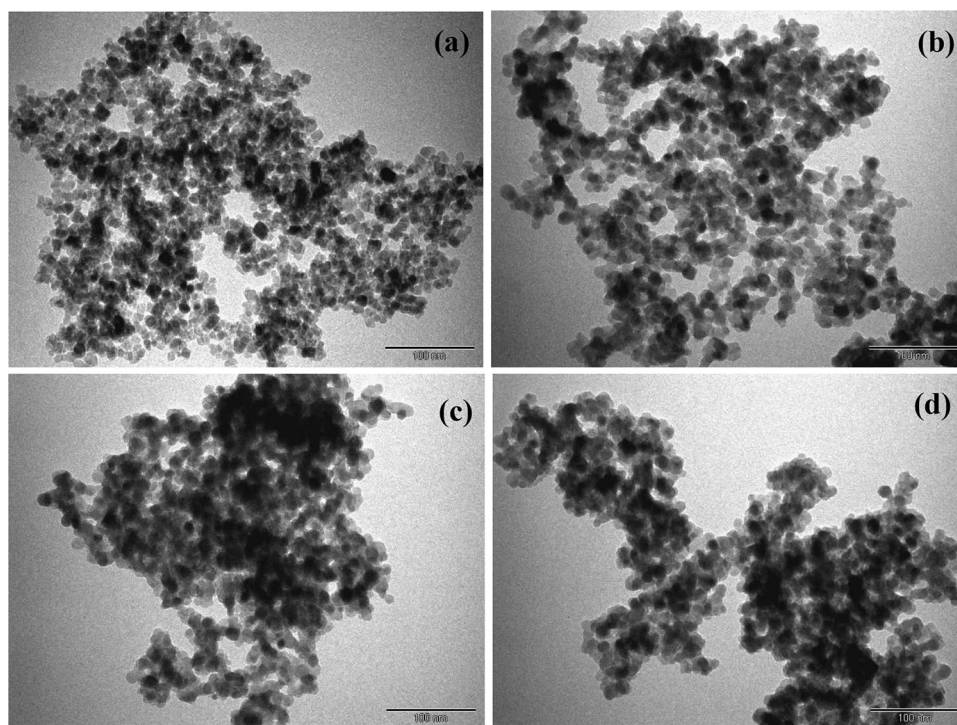


Fig. 6 Reflectance spectra of Mn–Ti nanocomposite for different Zn–M concentrations

rate of crystal growth, this is evidenced by the increased darkness of granules.

3.2 Optical Properties

3.2.1 Optical Property of Mn–Ti Composite

Optical reflectance spectra of Mn–Ti nano-composite samples for different Zn–M concentrations in the wavelength range 200–1600 nm is shown in Fig. 6. The samples showed

reflectance solely in the visible domain, while for Mn–Ti composites not only present strong reflectance in the visible region [28]. But also the reflectance was displaced to visible region, especially as the amount of Zn–M increased, being the Mn50%–Ti composite with the higher absorption for such samples in UV region [29]. Meanwhile, the enhancement of absorption in the ultraviolet region of Mn–Ti nanocomposite samples were obtained by increasing Zn–M concentrations. It can be seen that all samples were strong reflectance in the UV region [30]. The reflectance edge of Mn–Ti composites moved to longer wavelength in comparison with pure TiO₂ indicating the band gap was decreased by the incorporation Zn–M concentrations. The significant increase of red shift in reflectance edge is resulting from the narrow band gap by the incorporation Zn–M in TiO₂ band energy [11, 31]. For small amount of Zn–M concentrations in TiO₂, the absorption in visible region.

UV–Vis spectrums of Mn–Ti nano-composite samples for different Zn–M concentrations in the wavelength range 200–1600 nm is shown in Fig. 7. Nano-composite samples have a few absorbance in the UV–Vis region, which it will be increased by adding Zn–M and TiO₂ then has expanded to shorter wavelengths. The Mn50%–Ti composite showed the higher absorbance; this may be due to a good interaction between Zn–M and TiO₂ generating more stable hollow-electron pairs [32–35]. The absorption edge of Mn–Ti nanocomposite samples at a wavelength of around 378 nm. It is also observed that the positions of the fundamental absorption edge and the cutoff wavelength shift towards red as the

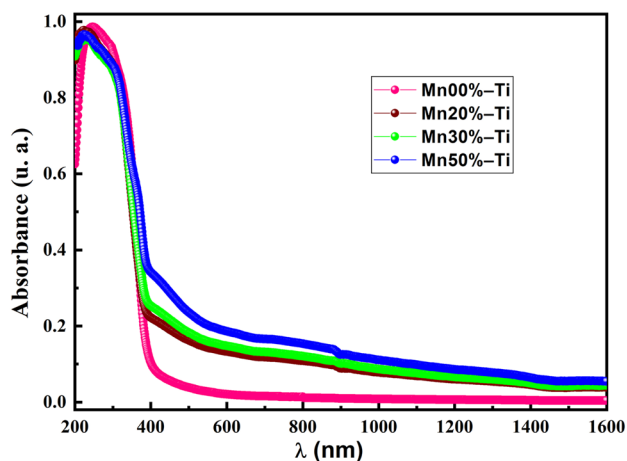


Fig. 7 UV-Vis-IR absorption spectra of Mn-Ti nanocomposite for different Zn-M concentrations

content of Zn-M increases. It appears that a part of Zn-M concentrations is responsible for the increase in the concentration of non-bridging oxygen due to which this shift is obtained [12, 14].

The optical band gap for Mn-Ti nano-composite samples for different Zn-M concentrations was evaluated using $(\alpha h\nu)^2 = A(h\nu - E_g)$, where A is a constant, $h\nu$ the photon energy and E_g is the energy band gap [14]. A Tauc plot can be drawn of $(\alpha h\nu)^2$ versus $h\nu$. The band gap of anatase TiO_2 nanoparticles is 3.32 eV, whereas band-gap of Mn-Ti nano-composite is increased to 3.30 eV (Fig. 8). The nano-composite prepared by sol-gel method has a high optical band gap with the value of 3.30 eV, which is comparable to the value reported for the composite material elaborated by sputtering [36].

The Table 2 summarizes the deduced values of the band gap of the different evaluated nano-composite samples; corroborating a low energy bandwidth for Mn00%-Ti and Mn50%-Ti composites. Thus, it would be expected that materials samples with a band-gap round 2.8 eV would

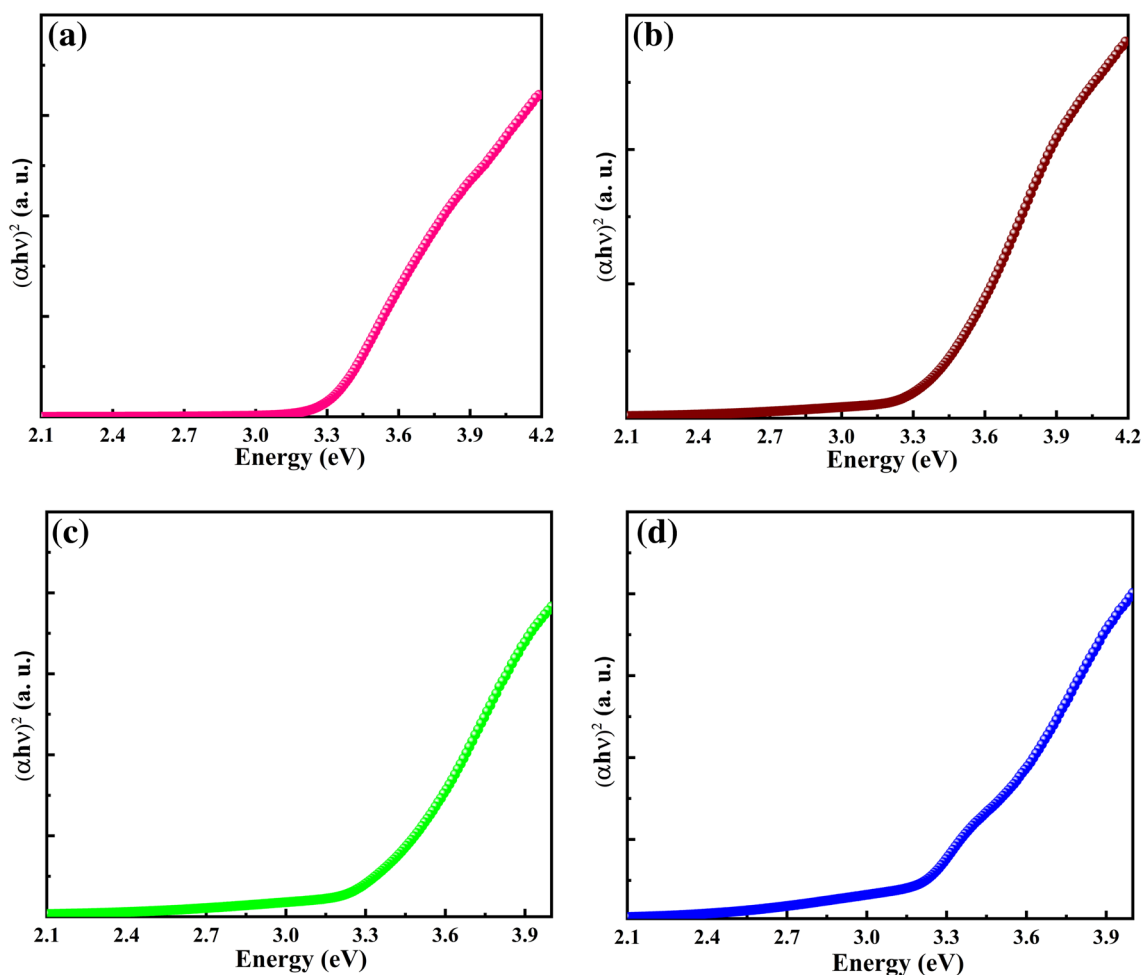


Fig. 8 The E_g spectra of of of **a** Mn00%-Ti, **b** Mn20%-Ti, **c** Mn30%-Ti, and **d** Mn50%-Ti nanocomposite

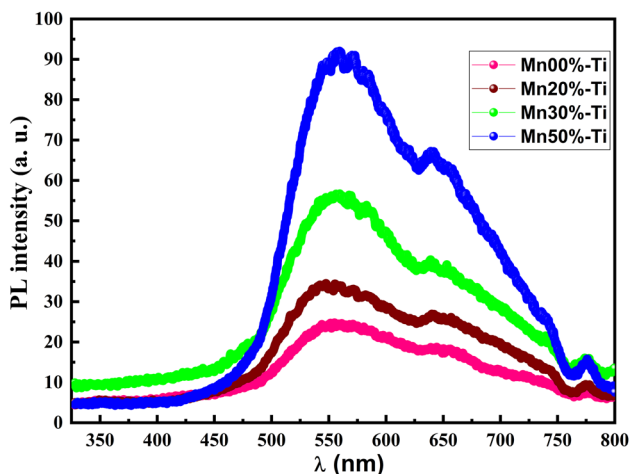
Table 2 The optical band gap values of Mn–Ti nanocomposite for different Zn–M concentrations

Zn–M doping concentrations (at.%)	0.0	20	30	50
Optical band gap (eV)	3.34	3.33	3.31	3.30
Crystallite size (nm)	10.33	14.20	15.10	27.00

have improved catalytic performance in the visible domain. It is clear that the band-gap decreases with increasing Zn–M contents in TiO₂ materials, which reflects the change in the electronic structure of the anatase TiO₂ [37]. This decrease is due to the interactions between Zn–M nanoparticles and anatase TiO₂ materials. In addition, this reduction in band-gap can be related to the increasing in the density of defect states [15]. The widening or increase in band-gap is attributed to the well-known Burstein–Moss band filling effect [26–30]. The Zn–M materials showed a large responsibility on the absorbance and energy gap of the Mn–Ti nanocomposites samples.

3.2.2 Photoluminescence Properties of Composite

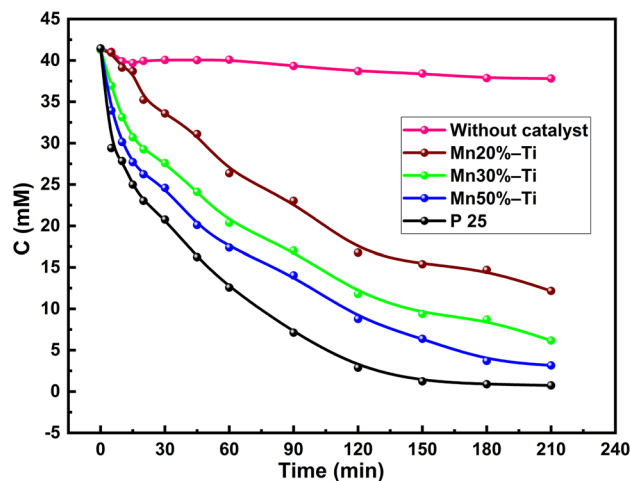
PL measurements were conducted in order to study the mechanism of the charge carrier recombination and energy transfer processes in the Mn–Ti nano-composite samples compared with anatase TiO₂. Figure 9 shows the typical PL spectra of pure anatase TiO₂ and of Mn–Ti nano-composite for different Zn–M concentrations at 77 K, excited with the UV laser pulses at 325 nm. The PL spectrum shows a strong luminescence, high yellow emission at 563 nm, at 640 nm and at 774 nm are observed from the Mn–Ti nano-composite samples [26]. The PL peak at 563 nm is known to originate

**Fig. 9** PL spectra of Mn–Ti nanocomposite for different Zn–M concentrations at 77 K

due to oxygen vacancies with one or two trapped electrons [38]. Room-temperature PL studies for nanostructured TiO₂ were reported in several works. Serpone et al. [37] examined the PL of anatase TiO₂ colloidal particles with different mean sizes, and found that observed PL occurs from the shallow trap levels located between 0.41 and 0.64 eV below the conduction band (CB). The intensity of Mn–Ti spectra are significantly increased as compared to that of the pristine anatase TiO₂ with increasing concentration of Zn–M. This result suggests that the incorporation of Zn–M sheets to the composite materials leads to improvement of its luminescence [7]. It can be seen that the increase in luminescence reaches ~80% of the initial emission of Mn00%–Ti composite, indicating that the dissociation of excitons occurs in Mn–Ti composites and increases with the Zn–M concentration [13]. This result obviously gives prominence to the interface between ZnO materials and TiO₂ in the charge dissociation process. Another possible cause of this charge dissociation difference may be the consequence of the uniform dispersion of Zn–M materials on the surface of the composite sample [7]. The PL intensity of Mn00%–Ti composite are weaker than Mn–Ti composites. It is confirmed the improved separation of electron–hole pairs, and the prolonged lifetime of carriers, which is contributed to the improved photocatalytic activity.

3.3 Photo-Catalytic Activities of Mn–O–Ti Nano-composites

Figure 10 shows the photo-catalytic activities of Mn–Ti nano-composite for different Zn–M concentrations on the degradation of MO. These results obtained of the composite samples shows an effective photo-degradation process.

**Fig. 10** Photocatalytic activities of Mn–Ti nanocomposite for different Zn–M concentrations on the degradation of MO under the irradiation of UV light

Thus, it is concluded that these composite materials are non-active under visible light, and that degradation of Mn-Ti is mainly due to its sensitization in the presence of the Zn-M materials [39]. Thereby, the ejection of electrons from the excited ZnO to the conduction bands of the Mn-Ti composite leading to its further degradation. From these subsequent experiments, it is expected that Mn00%-Ti sample exhibit very low photo-catalytic activity UV irradiation. The TiO₂ is known to be active only under UV light because of its band gap, but the Mn50%-Ti composite with incorporation of the Zn-M in TiO₂ nano-materials could be an effective technique to progress the excitation, and its photo-catalytic activity, with UV irradiation [40]. In the case of Mn50%-Ti composite sample, the degradation percentage was increased as the amount of Zn-M materials was increased. The highest photocatalytic activity was obtained with Mn50%-Ti composite sample, these results may be associated to better absorbance obtained in the UV range due to the synergy between Zn-M and TiO₂, probably due to the overlap of their bands since they intimately interact [32].

The photo-catalytic activity is related with the band-gap obtained previously in both composites (Mn00%-Ti and Mn50%-Ti, shown further), which allows greater photo-catalytic activity under UV light compared to P25 (as a reference photo-catalyst) [27, 30]. Such results confirm that there is a synergistic interaction between ZnO doped and TiO₂, which depends on the morphology and the proportion of Zn-M in each Mn-Ti composite. The adequate percentage of TiO₂ materials at the nano-composites depend on the typical of ZnO materials, in this case the morphology and the size played an important role. Therefore, it was obligatory higher content of Zn-M materials. In the case of Mn50%-Ti composites; they have high size and low band-gap compared with anatase TiO₂, which led to obtain better photo-catalytic activity with high percentage of Zn-M [7, 41].

MO degradation efficiency achieved by the as-prepared catalysts is presented in Fig. 11. As can be seen, when no catalysts are added to the solution, MO degradation efficiency was 6.19%; however, with the addition of the as-prepared Zn-M based catalysts, the photo-catalytic efficiency after 150 min of irradiation was about 76, 88, and 96% for Mn00%-Ti, Mn30%-Ti and Mn50%-Ti, respectively. In fact, the highest photo-degradation of 96% of the MO by the Mn50%-Ti composite sample was achieved in 210 min [42].

For the Zn-M containing samples, Mn50%-Ti composite showed high activity efficiency from the beginning to the end of the evaluated irradiation times. In general, the Zn-M materials containing samples showed higher photo-catalytic activity in comparison with the anatase TiO₂ sample [43]. In this study, the results from photo-degradation experiments indicate that low concentration of nanoparticles (20% of Zn-M) can effectively enhance the photocatalytic activity of the anatase TiO₂ catalyst. Thus, these experimental findings of structural,

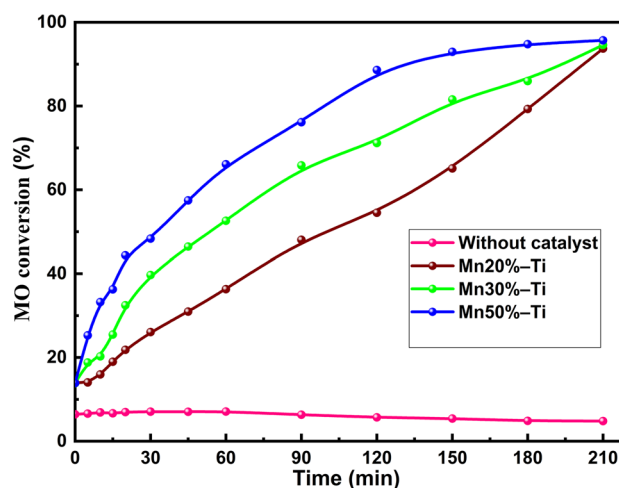


Fig. 11 MO conversion as a function of UV irradiation time in the presence Zn-M concentrations

optical and photo-catalytic property of Mn-Ti composites samples would be useful in their optoelectronics applications.

4 Conclusion

In this paper for controlling the Zn-M nanoparticles incorporated in TiO₂ composite, Mn-Ti nano-composite for different Zn-M concentrations were prepared in two steps. The composites samples derived from TiO₂ and Zn-M nanoparticles elaborated by the sol-gel method. Moreover, XRD, SEM and TEM analysis established the success synthesise of nano-composites. The absorption edge of Mn-Ti composite was found to be significantly shifted to longer wavelengths compared to anatase TiO₂ sample due to the reducing in the band-gap. The primary valuation band-gap decreases from 3.32 eV for pure anatase TiO₂ to 3.30 eV for Mn50%-Ti composite. Examination of the PL spectra excited by the UV laser pulses at 325 nm revealed the characteristic emission peaks attributed to the yellow luminescence from the oxygen vacancies with one or two trapped electrons. The composite system Mn-Ti is very active under UV irradiation. This photo-catalytic activity varies with the weight ratio of Zn-M concentration incorporated into TiO₂ composite. The Mn50%-Ti composite showed the highest photo-catalytic activity. Due to these characteristics, this allows our new composite to be a potential competitor as an UV filter for health and environment applications.

References

1. A. Fujishima, X. Zhang, Titanium dioxide photocatalysis: present situation and future approaches. *Comptes Rendus Chim.* **9**, 750–760 (2006)
2. S. Zhou, Y. Liu, J. Li, Y. Wang, G. Jiang, Z. Zhao, D. Wang, A. Duan, J. Liu, Y. Wei, Facile in situ synthesis of graphitic carbon

- nitride ($g\text{-C}_3\text{N}_4$)-N-TiO₂ heterojunction as an efficient photocatalyst for the selective photoreduction of CO₂ to CO. *Appl. Catal. B: Environ.* **158–159**, 20–29 (2014)
3. S. Horikoshi, H. Hidaka, N. Serpone, Environmental remediation by an integrated microwave/UV-illumination technique. *J. Photochem. Photobiol. A: Chem.* **159**, 289–300 (2003)
 4. Y. Paz, Application of TiO₂ photocatalysis for air treatment: patents' overview. *Appl. Catal. B: Environ.* **99**, 448–460 (2010)
 5. Y. Ma, X. Wang, Y. Jia, X. Chen, H. Han, C. Li, Titanium dioxide-based nanomaterials for photocatalytic fuel generations. *Chem. Rev.* **114**, 9987–10043 (2014)
 6. C. Li, Z. Sun, Y. Xue, G. Yao, S. Zheng, A facile synthesis of $g\text{-C}_3\text{N}_4/\text{TiO}_2$ hybrid photocatalysts by sol–gel method and its enhanced photodegradation towards methylene blue under visible light. *Adv. Powder Technol.* **27**(2), 330–337 (2016)
 7. L. Xu, G. Zheng, H. Wu, J. Wang, F. Gu, J. Su, F. Xian, Z. Liu, Strong ultraviolet and violet emissions from ZnO/TiO₂ multilayer thin films. *Opt. Mater.* **35**, 1582–1586 (2013)
 8. J. Yang, X. Zhang, H. Liu, C. Wang, S. Liu, P. Sun, L. Wang, Y. Liu, Heterostructured TiO₂/WO₃ porous microspheres: preparation, characterization and photocatalytic properties. *Catal. Today* **201**, 195–202 (2013)
 9. B. Wang, F.C. de Godoi, Z. Sun, Q. Zeng, S. Zheng, R.L. Frost, Synthesis, characterization and activity of an immobilized photocatalyst: natural porous diatomite supported titania nanoparticles. *J. Colloid Interface Sci.* **438**, 204–211 (2015)
 10. L. Shi, H. Shen, L. Jiang, X. Li, Co-emission of UV, violet and green photoluminescence of ZnO/TiO₂ thin film. *Mater. Lett.* **61**, 4735–4737 (2007)
 11. M.B. Askari, Z.T. Banizi, S. Soltani, M. Seifi, Comparison of optical properties and photocatalytic behavior of TiO₂/MWCNT, CdS/MWCNT and TiO₂/CdS/MWCNT nano-composites. *Optik* **157**, 230–239 (2018)
 12. M. Madani, K. Omri, N. Fattah, A. Ghorbal, X. Portier, Influence of silica ratio on structural and optical properties of SiO₂/TiO₂ nano-composites prepared by simple solid-phase reaction. *J. Mater. Sci.: Mater. Electron.* **28**, 12977–12983 (2017)
 13. K. Omri, L. El, Mir, Effect of manganese concentration on photoluminescence properties of Zn₂SiO₄:Mn nanophosphor material. *Superlattices Microstruct.* **70**, 24–32 (2014)
 14. K. Omri, I. Najeh, L. El, Mir, Influence of annealing temperature on the microstructure and dielectric properties of ZnO nanoparticles. *Ceram. Int.* **42**, 8940–8948 (2016)
 15. V. Loryuenyong, N. Jarunsak, T. Chuangchai, V. Buasri, The photocatalytic reduction of hexavalent chromium by controllable mesoporous anatase TiO₂ nanoparticles. *Adv. Mater. Sci. and Eng.* (2014). <https://doi.org/10.1155/2014/348427>
 16. Z. Antic, R.M. Krsmanovic, M.G. Nikolic, M. Marinovic-Cincovic, M. Mitric, S. Polizzi, M.D. Dramicanin, Multisite luminescence of rare earth doped TiO₂ anatase nanoparticles. *Mater. Chem. Phys.* **135**, 1064–1069 (2012)
 17. T. Homann, T. Bredow, K. Jug, Adsorption of small molecules on the anatase (1 0 0) surface. *Surf. Sci.* **555**, 135 (2004)
 18. S. Sain, J. Bhattacharjee, M. Mukherjee, D. Das, S.K. Pradhan, Microstructural, magnetic and optical characterizations of nanocrystalline Zn_{1-x}Mn_xO dilute magnetic semiconductors synthesized by mechanical alloying. *J. Alloys Compd.* **519**, 112–122 (2012)
 19. Z. Antic, M.R. Krsmanovi, M.G. Nikoli, G. Marko, M. Marinović-Cincović, M. Mitric, S. Polizzi, M.D. Dramićanin, Multisite luminescence of rare earth doped TiO₂ anatase nanoparticles. *Mater. Chem. Phys.* **135**, 1064–1069 (2012)
 20. P. Vlazan, D.H. Ursu, C. Irina-Moisescu, I. Miron, P. Sfirloaga, E. Rusu, Structural and electrical properties of TiO₂/ZnO core-shell nanoparticles synthesized by hydrothermal method. *Mater. Charact.* **101**, 153–158 (2015)
 21. C. Karunakaran, P. Vinayagamoorthy, J. Jayabharathi, Electrical, optical and photocatalytic properties of polyethylene glycol-assisted sol–gel synthesized Mn-doped TiO₂/ZnO core–shell nanoparticles. *Superlattices Microstruct.* **64**, 569–580 (2013)
 22. L. Kernazhitsky, V. Shymanovska, T. Gavrilko, V. Naumov, L. Fedorenko, V. Kshnyakin, J. Baran, Room temperature photoluminescence of anatase and rutile TiO₂ powders. *J. Lumin.* **146**, 199–204 (2014)
 23. Y. Chen, C. Zhang, W. Huang, C. Yang, T. Huang, Y. Situ, H. Huang, Synthesis of porous ZnO/TiO₂ thin films with superhydrophilicity and photocatalytic activity via a template-free sol–gel method. *Surf. Coat. Technol.* **258**, 531–538 (2014)
 24. V. Musat, A. Rego, R. Monteiro, E. Fortunato, Microstructure and gas-sensing properties of sol–gel ZnO thin films. *Thin Solid Films* **516**, 1512 (2008)
 25. C. Shifu, Z. Wei, L. Wei, Z. Sujuan, Preparation, characterization and activity evaluation of p–n junction photocatalyst p–ZnO/n–TiO₂. *Appl. Surf. Sci.* **255**, 2478–2484 (2008)
 26. B. Cullity, *Elements of X-Ray Diffraction* (Addison-Wesley, Menlo Park, CA, 1978)
 27. L.G. Devi, N. Kottam, B.N. Murthy, S.G. Kumar, Enhanced photocatalytic activity of transition metal ions Mn²⁺, Ni²⁺ and Zn²⁺ doped polycrystalline titania for the degradation of Aniline Blue under UV/solar light. *J. Mol. Catal. A: Chem.* **328**, 44–52 (2010)
 28. K. Oyoshi, N. Sumi, I. Umezumi, R. Souda, A. Yamazaki, H. Haneda, T. Mitsuhashi, Structure, optical absorption and electronic states of Zn⁺ ion implanted and subsequently annealed sol–gel anatase TiO₂ films. *Nucl. Instrum. Methods B.* **168**, 221–228 (2000)
 29. S.S. Kanmani, K. Ramachandran, Synthesis and characterization of TiO₂/ZnO core/shell nanomaterials for solar cell applications. *Renew. Energy* **43**, 149–156 (2012)
 30. N. San, A. Hatipoglu, G. Kocturk, Z. Cinar, Photocatalytic degradation of 4-nitrophenol in aqueous TiO₂ suspensions: theoretical prediction of the intermediates. *J. Photochem. Photobiol. A.* **146**, 189–197 (2002)
 31. K. Karthik, S. Kesava Pandian, N. Victor, Jaya, Effect of nickel doping on structural, optical and electrical properties of TiO₂ nanoparticles by sol–gel method. *Appl. Surf. Sci.* **256**, 6829–6833 (2010)
 32. J.F. Bertone, P. Jiang, K.S. Hwang, D.M. Mittleman, V.L. Colvin, Thickness dependence of the optical properties of ordered silica-air and air-polymer photonic crystals. *Phys. Rev. Lett.* **83**(2), 300–303 (1999)
 33. D. Kanakaraju, S. Ravichandar, Y.C. Lim, Combined effects of adsorption and photocatalysis by hybrid TiO₂/ZnO-calcium alginate beads for the removal of copper. *J. Environ. Sci.* **55**, 214–223 (2017)
 34. B.A. Sava, A. Diaconu, M. Elisa, C.E.A. Grigorescu, C. Vasiliu, A. Manea, Structural characterization of the sol–gel oxide powders from the ZnO–TiO₂–SiO₂ system. *Superlattices Microstruct.* **42**, 314–321 (2007)
 35. X. Xiao, W. Wenjun, L. Shuhong, Z. Wanquan, Z. Dong, D. Qianqian, G. Xuexi, Z. Bingyuan, Investigation of defect modes with Al₂O₃ and TiO₂ in one-dimensional photonic crystals. *Opt. Int. J. Light Electron Opt.* **127**(1), 135–138 (2016)
 36. S.K. Sinha, T. Rakshit, S.K. Ray, I. Manna, Characterization of ZnO–SnO₂ thin film composites prepared by pulsed laser deposition. *Appl. Surf. Sci.* **257**, 10551–10556 (2011)
 37. N. Serpone, D. Lawless, R. Khairutdinov, Size effects on the photophysical properties of colloidal anatase TiO₂ particles: size quantization versus direct transitions in this indirect semiconductor? *J. Phys. Chem.* **99**, 16646–16654 (1995)
 38. J. Tian, L. Chen, J. Dai, X. Wang, Y. Yin, P. Wu, Preparation and characterization of TiO₂, ZnO, and TiO₂/ZnO nanofilms via sol–gel process. *Ceram. Int.* **35**, 2261–2270 (2009)

39. E. Rego, J. Marto, P. São, J.A. Marcos, Labrincha, Decolouration of Orange II solutions by TiO₂ and ZnO active layers screen-printed on ceramic tiles under sunlight irradiation. *Appl. Catal. A-Gen.* **355**, 109–114 (2009)
40. R.J. Barnes, R. Molina, J. Xu, P.J. Dobson, I.P. Thompson, Comparison of TiO₂ and ZnO nanoparticles for photocatalytic degradation of methylene blue and the correlated inactivation of gram-positive and gram-negative bacteria. *J. Nanopart. Res.* **15**, 1432–1442 (2013)
41. D.L. Liao, C.A. Badour, B.Q. Liao, Preparation of nanosized TiO₂/ZnO composite catalyst and its photocatalytic activity for degradation of methyl orange. *J. Photochem. Photobiol. A* **194**, 11–19 (2008)
42. W.-Y. Choi, J. Chung, C.-H. Cho, J.-O. Kim, Fabrication and photocatalytic activity of a novel nanostructured TiO₂ metal membrane. *Desalination* **279**, 359–366 (2011)
43. C.A. Aggelopoulos, M. Dimitropoulos, K. Govatsi, L. Sygellou, C.D. Tsakiroglou, S.N. Yannopoulos, Influence of the surface-to-bulk defects ratio of ZnO and TiO₂ on their UV-mediated photocatalytic activity. *Appl. Catal. B: Environ.* **205**, 292–301 (2017)